Extreme Gradients in the Nocturnal Boundary Layer: Structure, Evolution, and Potential Causes

BEN B. BALSLEY, ROD G. FREHLICH, MICHAEL L. JENSEN, AND YANNICK MEILLIER

CIRES, University of Colorado, Boulder, Colorado

ANDREAS MUSCHINSKI

CIRES, University of Colorado, and NOAA/Environmental Technology Laboratory, Boulder, Colorado

(Manuscript received 22 July 2002, in final form 22 January 2003)

ABSTRACT

During the Cooperative Atmosphere–Surface Exchange Study-1999 (CASES-99) campaign in southeastern Kansas in the fall of 1999, the University of Colorado's Cooperative Institute for Research in Environmental Sciences (CIRES) made a series of vertical profiling measurements using the CIRES tethered lifting system (TLS). The results reported here began during a period when the nocturnal boundary layer (NBL) was characterized by a low-level jet (LLJ) peaking at 120 m and a temperature profile that increased smoothly with height to a point slightly above the height of the LLJ peak. Then, within a period of less than 30 min, the character of the NBL changed abruptly, with the breakdown of the well-defined LLJ and the appearance of a surprisingly steep temperature change of some 3.5 K around 180–190 m AGL. Part of this inversion was extremely sharp, with the steepest portion showing a temperature change of 1 K over an altitude range of only 5 cm, corresponding to a vertical temperature gradient in excess of 20 K m^{-1}. The general shape of this steep gradient was maintained—albeit with slightly reduced values—for at least 20 min. It is understood that the magnitude of the steepest portion of this gradient exceeds all previously observed atmospheric gradients by over an order of magnitude, although comparable gradients—albeit under very disparate conditions—have been observed in the ocean.

A second surprising feature apparent in these results was the steepness of the gradients in turbulence structure at the top of the NBL and within the residual layer (RL), the region above the NBL that is usually slightly stably stratified and extends upward to the height marked by the vestiges of the previous day's capping inversion. At the NBL top, energy dissipation rates and temperature structure parameters dropped sharply by more than one order of magnitude over a distance of only a few meters. At higher altitudes within the RL, a 60-m-thick region of very weak turbulence was observed. This low-turbulence region also exhibited sharp edges, where energy dissipation rates and temperature structure parameters changed by at least an order of magnitude over vertical distances of only a few meters.

1. Introduction

In several respects, the nocturnal boundary layer (NBL), sometimes referred to as the stable boundary layer (SBL), is more difficult to understand than the daytime convective boundary layer (CBL). While the CBL is controlled largely by surface heating and convective turbulence, the NBL is characterized by strong radiative cooling, significant stratification, and sporadic turbulence. Additional complicating factors include a continuously evolving wind structure, as well as a rich collection of propagating atmospheric gravity waves (Mahrt et al. 1979; Mahrt 1998; Stull 1988; Kaimal and Finnigan 1994). Our ability to understand the NBL is further limited by the paucity of systematic high-vertical-resolution measurements from the surface to well above the ''top'' of the NBL (Mahrt et al. 1979).

The turbulent structures of the NBL have been studied using instrumented towers (Garratt 1981; Nieuwstadt 1984a,b; Gossard et al. 1984; Smedman 1988; Smedman et al. 1995), instrumented aircraft (Mahrt 1985; Mahrt and Gamage 1987; Muschinski and Wode 1998), acoustic sounders (Gossard et al. 1984; Smedman 1988), and Frequency-Modulated Continuous Wave (FMCW) radars (Gossard et al. 1984; Eaton et al. 1993). While the daytime boundary layer is often quasi-stationary, the NBL often does not reach equilibrium (e.g., Wyngaard and Kosovic 1994). In spite of this, the assumption of a quasi-stationary stable boundary (e.g., Zilitinkevich and Mironov 1997) sometimes provides realistic estimates of the equilibrium depths (e.g., Handorf et al. 1999). Typical equilibrium depth estimates of the NBL

Corresponding author address: Dr. Ben B. Balsley, CIRES, University of Colorado, Campus Box 216, Boulder, CO 80309-0216.
E-mail: balsley@cires.colorado.edu

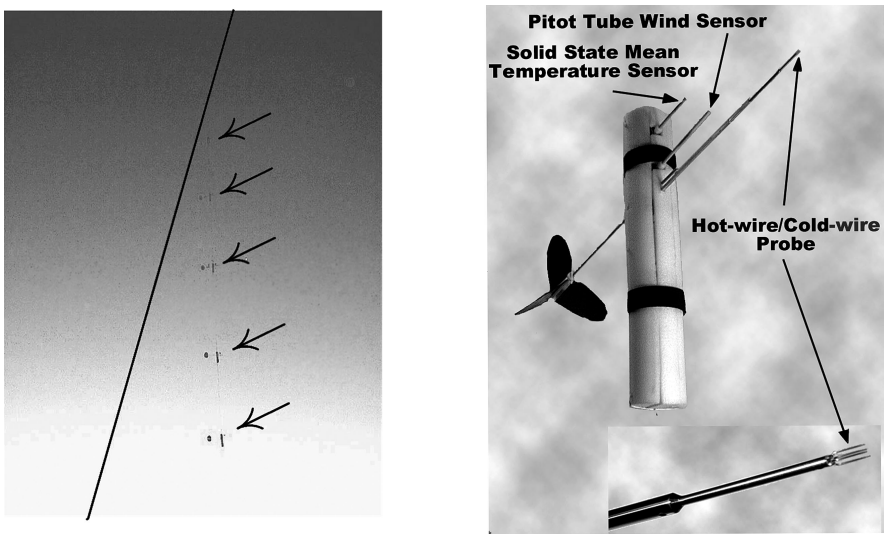

FIG. 1. (left) Photograph of five turbulence probe packages suspended at 6-m intervals below the CIRES TLS during CASES-99. The kite is flying well above the top of the photograph, and the tether is visible as a computer-enhanced straight line to the left of the probes, which are indicated by arrows. (right) Details of a single turbulence sensor package shown in the left.

range from tens of meters to a few hundred meters. Additional useful general discussions of various aspects of NBL characteristics discussed herein can be found in Mahrt et al. (1979), Stull (1988), and Mahrt (1998).

One phenomenon that results from the nonstationary nature of the NBL is the low-level jet (LLJ; Blackadar 1957; Stull 1988; Smedman et al. 1995; Whiteman et al. 1997). The classical explanation of the LLJ (Blackadar 1957) takes into account the inertial oscillations induced by the mechanical decoupling of the lower troposphere from the ground around sunset under clear skies, that is, when the formation of a ground-based inversion leads to a relatively sudden decrease of the eddy viscosity (Stull 1988, section 6.4.5). The spatiotemporal patterns of the LLJ are relatively complicated but have been successfully reproduced by means of simple analytical models (e.g., Kottmeier 1978; Jacobi and Roth 1995). The LLJ, on the other hand, is not an ever present feature of the NBL. However, when it was present during the Cooperative Atmosphere–Surface Exchange Study-1999 (CASES-99), the maximum wind speed of the LLJ was typically between 7 and 10 m s^{-1} and the LLJ peak was located around 100 m above ground level (Banta et al. 2002).

2. Approach

In the following sections, we describe high-resolution in situ observations of the NBL made using the Cooperative Institute for Research in Environmental Sciences (CIRES) tethered lifting system (TLS) during CASES-99. CASES-99 was a multi-instrumented field campaign in southeastern Kansas approximately 40 km east of Wichita that involved both airborne and tower-based in situ sensors and additional remote sensing instruments such as UHF radars, an FMCW radar, lidars, and sodars (Poulos et al. 2002). The experiment was designed to study the structure and dynamics of the nighttime stable boundary layer. The in situ instrumentation component included the CIRES TLS, which basically involves lofting either a kite or an aerodynamic balloon (kites for moderate to strong wind conditions; balloons for low wind conditions) to carry a suite of lightweight instruments from the ground up through the first few kilometers of the atmosphere (Balsley et al. 1998; Eaton et al. 2000; Muschinski et al. 2001). A similar system to measure turbulence and cloud microphysics in the lower troposphere has been described by Siebert et al. (2003). Reviews on the state-of-the-art of atmospheric turbulence measurements have been given by Oncley (1999) and Muschinski and Lenschow (2001).

For CASES-99, the TLS instrumentation included a ''basic meteorological payload'' (BMP) that archived 1-s values of temperature, pressure, humidity, wind speed and direction, and various ''housekeeping'' data. As illustrated in Fig. 1, up to five additional ''turbulence'' payloads separated vertically by preselected spacings could be attached above or below the BMP. Each turbulence payload archived high-frequency (200 Hz) fluctuations of temperature and wind speed using cold-wire and hot-wire sensors, respectively. Each payload also carried conventional low-frequency sensors (e.g., a Pitot tube, a solid-state temperature sensor, and a piezo-electric pressure sensor) for sampling mean wind speed, temperature, and pressure, along with a three-axis tilt sensor and a magnetic compass. Separate archiving for each payload package was accomplished

using onboard digital flash-memory storage, with data downloads to disk occurring when the packages were brought down to the ground at the end of each night of operation [for further details see Frehlich et al. (2003)].

We present herein TLS measurements made in conjunction with a variety of other remote and in situ measurements provided by other CASES-99 instruments to document an unusual sequence of events that occurred during the early morning hours of 21 October 1999. The period began with a well-developed LLJ having maximum wind speeds of about 14 m s^{-1} at an approximately 120-m altitude. Within a period of much less than an hour, around 0730 UTC (UTC = LST + 5 h), the wind speed profile evolved from a narrow LLJ into a profile that increased with height from the ground to a point somewhat higher than the earlier-present LLJ peak, with roughly constant wind speed (9–12 m s^{-1}) above that height to at least 2500 m (as determined from nearby high-resolution radiosonde wind profiles). TLS temperature measurements made during the period marking the change in the wind profile document the development of an extremely steep positive temperature gradient near 180–190 m that remained for at least the next 20 min and possibly much longer. Appreciably enhanced radar returns from the region of this steep temperature gradient were evident on records of both the University of New Hampshire's FMCW radar located about 1 km east-northeast of the TLS site and (possibly) on the nearby 915-MHz wind profiler at Beaumont, Kansas, some 12 km east of the main site.

Another notable feature of the NBL observed by TLS during this period was the surprisingly steep gradients in the turbulence profiles (C_T^2, the temperature structure constant and ε, the energy dissipation rate) in the residual layer (RL), the region above the NBL that is usually slightly stably stratified and extends upward to the height marked by the vestiges of the previous day's capping inversion. Energy dissipation rates and temperature structure parameters within the RL exhibited very steep vertical gradients, with more than an order of magnitude changes over vertical distance of just a few meters. In contrast to the large transitory turbulence fluctuations in the SBL, these steep gradient regions in the RL were not just transitory but rather were reasonably consistent features over many tens of minutes, and possibly longer. Their presence does not appear to be correlated with presence/absence of the observed steep inversion.

3. Overview of atmospheric conditions during the night of 20–21 October 1999 (UTC)

Surface winds during the night of 20–21 October 1999 (UTC) were approximately out of the south-southwest at 3–4 m s^{-1}. Surface temperatures decreased systematically from 17°C just after sunset to 6°C near dawn. Surface pressure decreased from 973 mb near sunset to 971 mb just before dawn. No precipitation was recorded during this period, and the relative humidity increased through the night from about 40% to 80%.

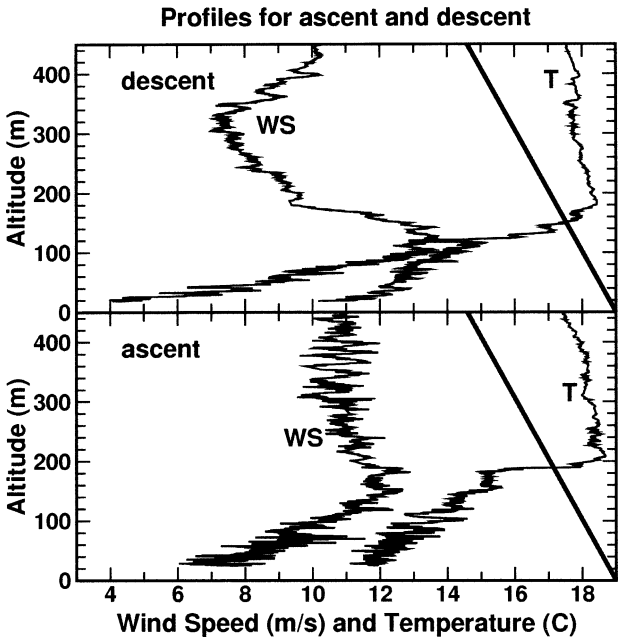

FIG. 2. TLS profiles of wind speed and temperature obtained from turbulence package 2 for two separate periods: (upper) 0614–0636 UTC; (lower) 0713–0731 UTC, on the night of 21 Oct 1999 during CASES-99. The left-hand profile in both denotes wind speed (WS), while the right-hand profile in both instances denotes temperature (T). The straight line to the right-hand side of each plot depicts the 9.8 K km^{-1} dry adiabatic lapse rate for reference.

During the night of 20–21 October 1999, intensive observation period (IOP) 9, six TLS ascents/descents were made between 0145–1215 UTC. The highest altitude of 500 m was reached around 0600 UTC. The remaining ascents/descents were made only to between 150–450 m, because most of the interesting dynamics were being reported by other observers in this lower height range. Since winds aloft were moderate, ranging between 5–14 m s^{-1} over the course of the evening, a kite was chosen to loft the instruments.

TLS profiles of wind speed and temperature for two separate periods during the night of 21 October 1999 are presented in Fig. 2. The wind speeds derived from the hot-wire probes that are presented herein have been carefully calibrated against laboratory standards and compared with remotely sensed wind profiles during CASES-99 (R. Coulter 2001, personal communication). The hot-wire velocity measurements have an absolute accuracy typically better than 1 m s^{-1}, while the accuracy of the slope of the calibration curve is better than 5%. Similarly, the cold-wire temperature probe data have also been carefully calibrated and have been shown to have an absolute accuracy of ± 0.5 K, while the accuracy of the slope of the calibration constant is better than 2%. Both the hot- and cold-wire sampling instruments and their calibration procedures are described in

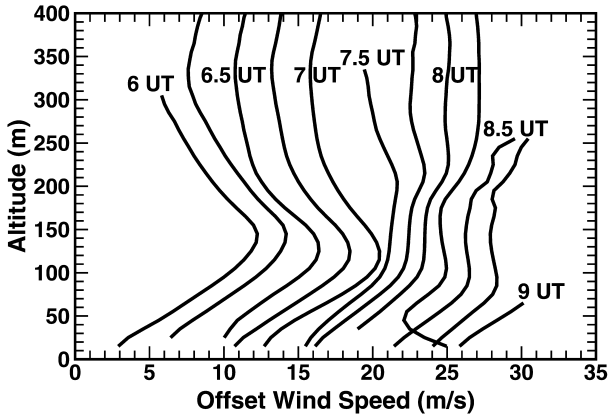

FIG. 3. A 3-h series of vertical profiles of horizontal velocity from the NOAA HRDL for the period centered on the time of appearance of the steep temperature gradient in Fig. 5. Profiles are 15-min averages centered on the times indicated (data provided with the assistance of R. Newsom 2002, personal communication).

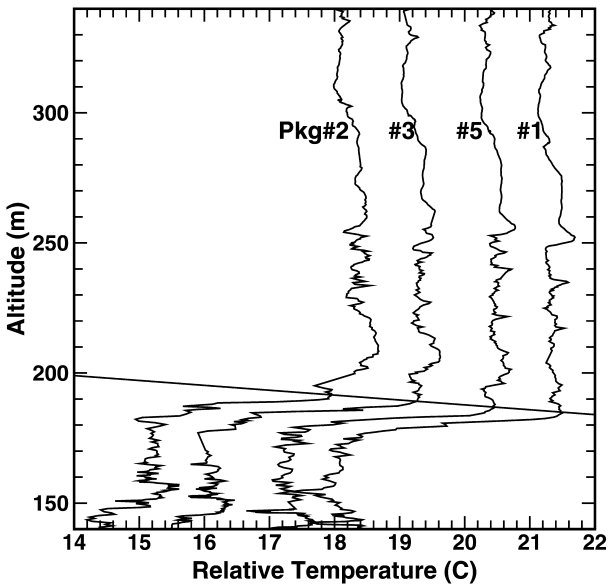

FIG. 4. One-second-averaged values of high-resolution TLS temperature profiles recorded by four individual cold-wire turbulence probes during the 0713–0731 UTC ascent on 21 Oct 1999. The temperature data on each sensor was recorded as that sensor passed upward through the region with a vertical velocity of 0.4 m s^{-1}. The occasional (straight line) data gaps in each profile (e.g., between 170–180 m on the package 3 profile) arise every 180 s when the data were being archived. Probe separation was 6 m and the top-to-bottom probe sequence was 2, 3, 5, and then 1. Package 2 temperature values are correct; values for the consecutive profiles have been incremented by 1.5 K for viewing facility. The sloping straight line indicates an *apparent* downward motion of the profile structure near the top of the temperature inversion.

Frehlich et al. (2003) that also appears in this special issue.

The upper set of profiles shown in Fig. 2 was obtained during a descent of the kite platform between 0614 and 0636 UTC, and shows a well-formed LLJ at a height of 120 m with a maximum wind speed of roughly 14 m s^{-1}; the corresponding temperature profile shows a moderate temperature increase with height up to about 190 m and a quasi-isothermal profile above that height. In the lower set of profiles, obtained during the subsequent ascent about an hour later, between 0713 and 0731 UTC, the narrow jet has essentially disappeared, while the temperature profile has developed a very sharp inversion at a height around 180–190 m. Markedly enhanced wind speed fluctuations above about 200 m are evident in the later profile relative to the earlier profile, suggesting a possible change in the dynamic properties of the region. Wind direction during this period (measured by TLS, but not shown here) was roughly south-southwesterly at the surface, veering gradually with increasing altitude to west-southwesterly above 150 m. Examination of earlier profiles indicates that the nocturnal jet first appeared about 0200 UTC, retained its general shape until just after 0715 UTC, at which point wind speeds above the earlier jet peak increased to produce an almost constant profile with height up to at least 2500 m.

Additional information on the evolution of the wind profile is shown in Fig. 3, which was derived from concurrent lidar wind speed profiles using the National Oceanic and Atmospheric Administration (NOAA) high-resolution Doppler lidar (HRDL). Except for the missing profile centered at 0715 UTC, this series of profiles depicts the evolution of the LLJ during the 3-h period centered on the time of occurrence of the steep temperature gradient just after 0700 UTC. Each profile has been averaged over a period ± 7.5 min of the time shown. The 0600 UTC profile has been correctly plotted using the horizontal scale of horizontal velocity while each succeeding profile has been offset from the previous profile by 2 m s^{-1} for each 15-min interval of separation.

4. A detailed study of the steep temperature gradient region around 180–190 m

In this section we examine the steep temperature gradient shown in the lower panel of Fig. 2 in greater detail. The rationale for this more detailed examination lies in the surprisingly large magnitude of the gradient, its apparent lifetime, and the apparent vertical motion of the structure.

Temperature profiles between 140–340 m obtained from the four separate high-frequency cold-wire temperature probes during the 0713–0731 UTC ascent are shown in Fig. 4. Vertical ascent/descent velocities for both this period and the subsequent descent (0731–0750 UTC) were constant at 0.4 m s^{-1}. For this flight, the probe packages were suspended beginning some 10 m below the kite platform with an interpackage separation of 6 m.

Examination of Fig. 4 shows a sharp temperature in-

crease with height near 180–190 m with a total temperature change of approximately 3.5 K. This sharp gradient was observed by all four vertically spaced sensor packages as they passed through the region at 15-s intervals. In addition to this pronounced gradient, a number of additional common features can be seen on all four profiles. Specifically, many of the sharp details beginning near the top of the gradient and extending to about 250 m appear to be quite similar. The single, smooth, quasi-sinusoidal feature between 255–330 m is also common to all profiles.

Careful examination of the height change of the sharp inversion shown in Fig. 4 shows an apparent downward motion of about 7 m in 45 s, that is, an *apparent* downward velocity of about 16 cm s^{-1}. This motion is indicated in Fig. 4 by the sloping solid line connecting similar structure at the top of the inversion on each profile. Given the available data, it is impossible to say whether the motion of this gradient surface is real or whether it arises from a slightly tilted (or a wavelike) gradient region advecting past the sensors at the wind speed. If this deduced motion arises from a tilted surface, then the tilt of that surface would have been less than 1°. Measurements of the height of the gradient during the subsequent descent some 20 min later shows that it remained within a very few meters of the height shown in Fig. 4, providing strong evidence that the motion is not a manifestation of a long-term vertical motion of the atmosphere. Thus, whether the deduced motion is the result of a slightly tilted surface advecting through the sensors, a wavelike surface propagating past the sensors, or to a true vertical wind, the effect is clearly short term, that is, on the scale of a few minutes. A cursory study considering the possibility that these slight vertical displacements could arise from the presence of a long-period gravity wave show that this possibility is remote for the following reasons: 1) there is no manifestation of a similar steep gradient in the wind speed measurements, and 2) there is no evidence of a secondary peak in the vertical temperature structure at higher height to suggest a vertical wavelength of less than a few hundred meters.

A more detailed plot of the steepest portion of the sharp temperature inversion appears in Fig. 5, where we have plotted the TLS temperature profile from the high-frequency cold-wire sensor on package 5 over a 10-cm interval between 183.3 and 183.4 m. This figure shows that the steep portion of the gradient region can be approximated by a straight line with a slope of 28 K m^{-1}. Similar, but slightly smaller, gradient values have been calculated for the other three packages. Note that this slope extends vertically for about 3 cm, and includes some 15–20 individual temperature measurements (circles). All four probes show similar results, with similar but slightly weaker gradients observed by all turbulence packages 20 min later during the descent. Since the accuracy of the slope of the temperature calibration is better than 2% for all the measurements we conclude

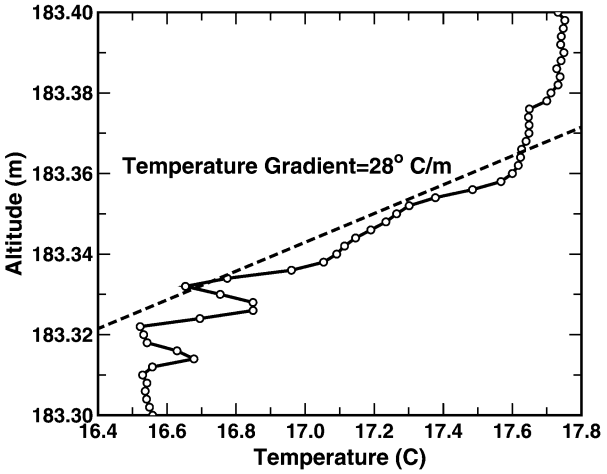

FIG. 5. Detailed view of the steep temperature inversion shown in Fig. 4 as measured at 200 Hz by package 5. Also shown is a linear approximation to the steepest region with a value of 28 K m^{-1}. Each independent data point is shown as an open circle.

that this surprisingly large magnitude of the temperature gradient is real.

That the steep gradient shown in Figs. 4–5 was also observed during the subsequent TLS descent (0731–0750 UTC), roughly that is, 20 min later, can be taken as an indication that the gradient extends horizontally well over 10 km. The mean value of the gradient over the full 3°–4° range during descent was comparable, while the steepest portions exhibited slightly reduced values relative to the earlier ascent. Clearly, however, the steep temperature gradients during either of these periods were much sharper than those observed earlier in the evening, when the well-formed LLJ was present.

It is also possible to estimate the minimum horizontal extent of the sharpest portions of the inversion (thickness $\approx$ 5 cm) shown in Fig. 5: assuming that the inversion was advected past the sensors by the 12 m s^{-1} mean wind and taking into account the 45 s required for all four sensors to traverse the inversion, it follows that the sharpest potion of the inversion must have had a horizontal extent of at least 500 m. The horizontal extent of these very sharp inversions will be important in the discussion of specular echo returns from vertically directed radar outlined in the discussion and conclusions section below.

5. Vertical profiles of turbulence structure parameters between 0713 and 0750 UTC

If the turbulence is locally stationary and isotropic over scales less than 5 to 10 m, then estimates of the temperature structure constant C_T^2 and energy dissipation rate ε can be obtained from estimates of the spectral level x_0 from 1-s sections of the high-frequency data. Here, we assume Taylor's frozen hypothesis, which is very accurate for these short sections of data and typical

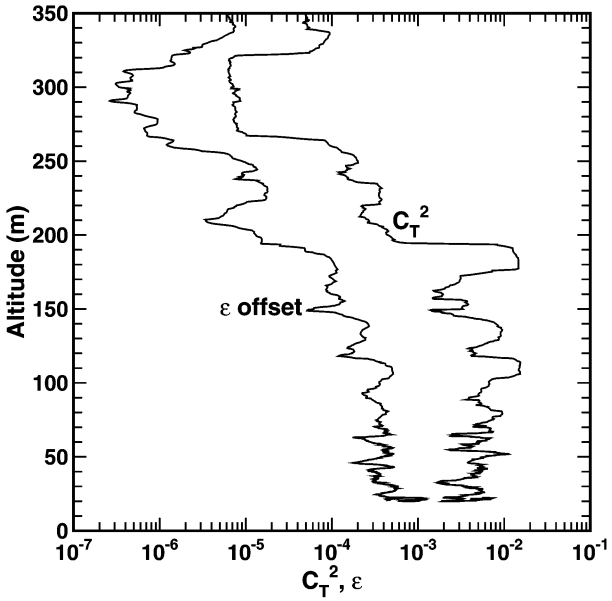

FIG. 6. Fifty-second smoothed profiles of both the temperature structure parameter (C_T^2) and the energy dissipation rate (ε) for the 0713–0731 UTC ascent of the TLS. (Units for C_T^2 and ε are, respectively, $m^{-2/3}$ K^2 and m^2 s^{-3}.) The ε profile in this figure has been offset to the left by an order of magnitude for viewing facility.

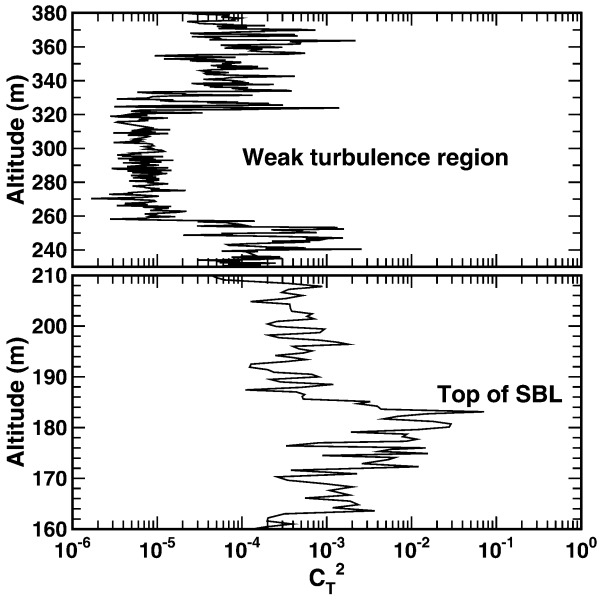

FIG. 7. Plots of 1-s values of C_T^2 that include details of the 255–325-m low-turbulence region (upper) and the 185-m region (lower) for the 0713–0731 UTC TLS ascent.

mean velocities (Frehlich et al. 2003). The accuracy of the 1-s estimates of the spectral level is better than 15%, which implies a 15% accuracy for C_T^2 and 22.5% accuracy for ε.

A 50-s running average profile of both the temperature structure parameter (C_T^2) and the energy dissipation rate (ε) obtained during the 0713–0731 UTC ascent are displayed in Fig. 6. At the 0.4 m s^{-1} ascent rate, a 50-s running average is equivalent to a 20-m smoothing function. These smoothed profiles provide a reasonable overview of the entire height range without including the intense smaller-scale fluctuations associated with nonsmoothed profiles (see, e.g., the following two figures). For reference, near-surface values of both C_T^2 and ε lie between 10^{-3}–10^{-2} $m^{-2/3}$ K^2 and m^2 s^{-3}, respectively.

One significant feature of Fig. 6 is the enhanced fluctuations in both turbulent quantities below about 70 m visible even in these smoothed profiles. A second feature is the occurrence of sharply defined decreases in C_T^2 with increased height near 185 and 255 m, and a similar increase in C_T^2 near 325 m. Similar features, albeit less well defined, can be seen in the profiles of ε. In all cases, these sharp changes are well in excess of an order of magnitude and, as we show in the following two figures, appear to occur over a vertical distance of a few meters.

To examine these steep features with better resolution we present two examples of 1-s-averaged temperature structure parameter (C_T^2) profiles in Figs. 7 and 8. Both figures include only the regions of sharp C_T^2 gradients, namely near 185 m (bottom), and the 255–325-m ''bite out'' in C_T^2 (upper). The results shown in Fig. 7 were obtained during the 0713–0731 UTC TLS ascent, while Fig. 8 shows comparable data obtained from the subsequent descent some 20 min later (0731–0750 UTC). Figure 7 exhibits the two sharp decreases in C_T^2 at heights of approximately 185 and 255 m as well as the

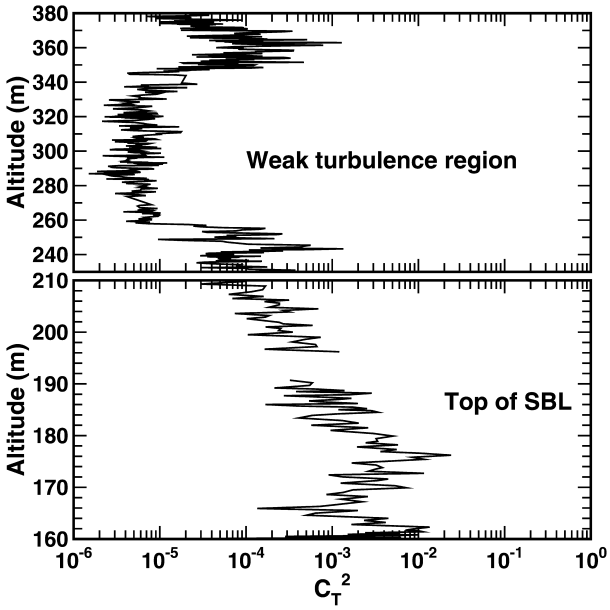

FIG. 8. Same as Fig. 6, except for the 0731–0750 UTC descent. The lack of data just above 190 m corresponds to the period when the turbulence data were being archived.

increase near 325 m. In Fig. 8 the bite-out region appears to have grown in height by about 20 m relative to the earlier region, while only a vestige of the lower ledge at 190 m remains. The transitions between C_T^2 levels apparent at the turbulent interfaces in the upper region are spatially abrupt and large in intensity in both figures. Moreover, this upper region exhibits roughly constant levels of rms C_T^2 fluctuations throughout, during both ascent and descent. The magnitude of the transition at 185 m in Fig. 6 is roughly a factor of 20 (13 dB), while the corresponding step at the higher interface is approximately a factor of 10 (10 dB). Taken together, and also taking into account the gradual decrease of C_T^2 with height between these two regions, Fig. 6 documents a change in C_T^2 level of more than three orders of magnitude ($\sim 10^{-2}$ to 10^{-5} m$^{-2/3}$ K^2) over a vertical scale of less than 100 m.

Note that the approximately 10-dB peak-to-peak magnitude of the C_T^2 fluctuations about the mean in these profiles is reminiscent of earlier observations of temporal fluctuation of turbulence levels (Gossard et al. 1984; Bezverkhniy et al. 1986, 1988; Frehlich 1992), and so appears to be consistent with the inherent variability of turbulence structures in general. This so-called ''global turbulence intermittency'' has been studied in detail by Mahrt (1989) and observed by others (e.g., Balsley et al. 1998; Frehlich et al. 1998; Eaton et al. 2000; Muschinski et al. 2000).

Comparison between Figs. 5 and 7 shows that the C_T^2 ledge near 185 m lies very close to the steep positive temperature gradient just above 183 m. As discussed below, this steep gradient marks the upper height of the SBL and the lower height of the RL. The higher bite-out region, on the other hand, does not appear to be associated with any such strong temperature gradient. However, the stability analyses discussed below show that the lower edge of this region ($\sim$255 m) lies just above a region of appreciable static stability, and low velocity shear, so that the gradient Richardson number (Ri) is quite large. This elevated region of high Ri along with observations of other similar regions above the SBL during CASES-99 appears to be related to the existence of one or more shallow inversion layers discussed by Kaimal and Finnigan (1994) and Mahrt (1998) that may be vestiges of earlier capping inversions.

Finally, it is important to point out that steep interfaces similar to those shown here for C_T^2 are equally apparent in concurrent profiles of ε. As indicated in Fig. 6, the steps are comparable in magnitude and height, but perhaps somewhat less steep. Except for the 30-s smoothed profile shown in Fig. 6, however, concurrent profiles of ε have not been included herein.

6. Stability analysis and identification of the heights of the stable boundary layer and the residual layer

In an attempt to better quantify the causal mechanisms responsible for the sharp gradients in the observed vertical turbulence structure during the 0731–0731 UTC ascent of the TLS, we present a stability analysis based on the high-resolution temperature, wind speed, and pressure profiles from that ascent. Vertical profiles of the potential temperature (θ), the buoyancy frequency parameter (N^2), the vertical wind shear parameter $(dU/dz)^2$, and the resulting gradient Richardson number [Ri $= N^2/(dU/dz)^2$] are presented and discussed in this section. These results, along with results from other CASES-99 datasets, have been included to better define the vertical extent of both the SBL, the RL, and the height of the capping inversion that defines the top of the RL. They are also important in examining the mechanisms responsible for the turbulence bite outs in Figs. 7 and 8.

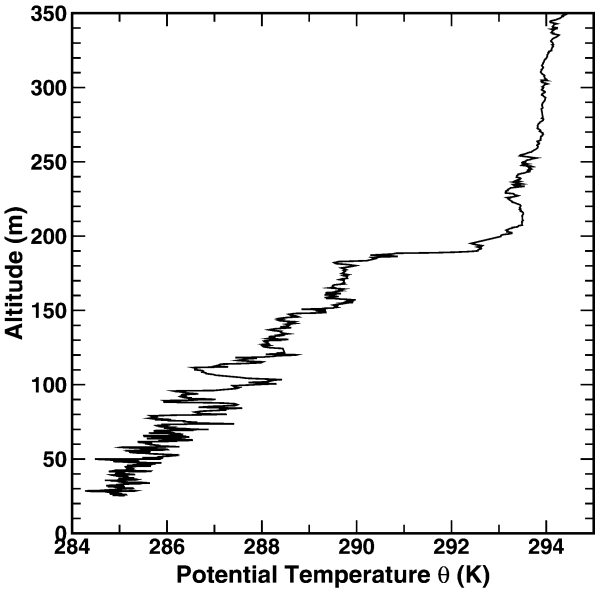

FIG. 9. Vertical profile of potential temperature obtained from 1-s values of the cold-wire temperature sensor and the pressure sensor on package 2 during the 0713–0731 UTC ascent.

A vertical profile of the potential temperature θ during the 0713–0731 UTC TLS ascent appears in Fig. 9. This profile was calculated from unsmoothed 1-s values of temperature and pressure. Calculated values of N^2 and $(dU/dz)^2$ from the same ascent are presented in Fig. 10. Note that we have computed only the shear in the *magnitude* of the horizontal wind and have ignored any directional shear. The rationale for this procedure is that total change in horizontal wind direction from the surface to 350 m was only some 30°, with the majority of the direction change occurring in the first 150 m, that is, well within the SBL. It is, further, important to point out that the N^2 and $(dU/dz)^2$ profiles have not been calculated directly from the potential temperature and wind speed data, but rather from fifth-order polynomial fits to three overlapping sections in both these datasets. This procedure provides a convenient method of representing the primary features in the measured profiles and of reducing the effects of the intense smaller-scale

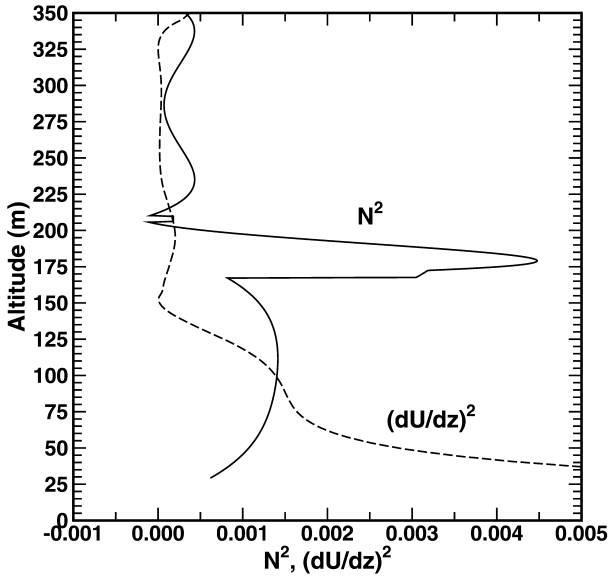

FIG. 10. Profiles of N^2 and $(dU/dz)^2$ obtained for the 0713–0731 UTC ascent using three overlapping polynomial fits to the observed temperature profile (for N^2 determination), and for the wind speed profile [for determining $(dU/dz)^2$]. Note that the accuracy of either of these quantities are questionable near 170 and 215 m, since these heights correspond to the overlap heights of the individual polynomial fits of both the wind and temperature profiles used to calculate N^2 and $(dU/dz)^2$.

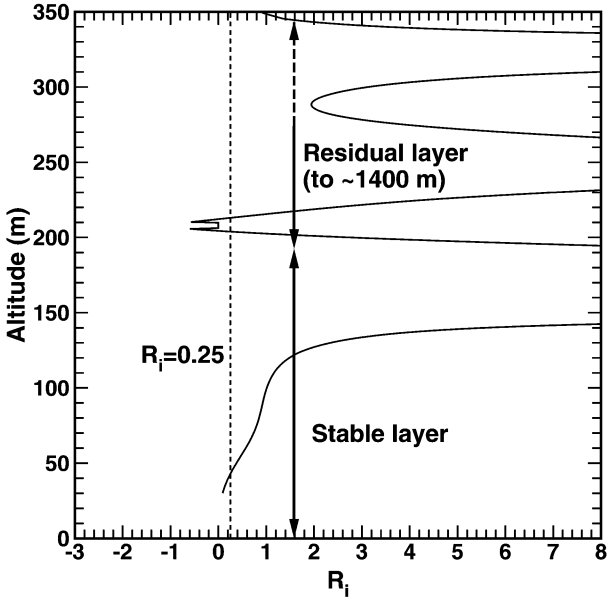

FIG. 11. Richardson number profile obtained using the N^2 and $(dU/dz)^2$ values in Fig. 10. The vertical line delineates the 0.25 value if Ri, while the various regions of the NBL and free atmosphere are suggested by the vertical arrows. See Fig. 11 caption for comments on Ri values around 170 and 215 m.

fluctuations contained in both temperature wind speed profiles (see, e.g., Fig. 2).

The resulting plot of the gradient Richardson number Ri appears in Fig. 11. In this figure the horizontal axis has been scaled to illustrate details of values of Ri less than 8, so that Ri values in the height ranges centered on 150, 250, and 325 m are off scale. We have chosen this procedure to better examine the unstable boundary condition Ri = 0.25. To have included the full extent of Ri, the horizontal scale would have to have been extended by much more than an order of magnitude (maximum Ri values in the 150-, 250-, and 325-m regions extend, respectively, to 170, 170, and 230). Considerable detail in the Ri = 0.25 region would have been compromised in presenting such an all-inclusive figure.

Using the above results in conjunction with results available from other CASES-99 datasets, it is relatively easy to delineate the height ranges of both the SBL and the RL discussed earlier. SBL height has been variously defined as the height at which turbulence levels drop to a small fraction of surface levels (Stull 1988; Kaimal and Finnigan 1994), the height of the peak of the velocity profile (Kaimal and Finnigan 1994), the height at which the potential temperature profile become almost adiabatic (Stull 1988; Kaimal and Finnigan 1994), and the height above which sodar echoes are absent (Kaimal and Finnigan 1994). Examination of the data available from the CASES-99 dataset for the period around the 0713–0731 UTC TLS ascent shows the height of the top of the strong inversion (~200 m), the height of the jet maximum (~190 m), the height at which turbulence decreases to about 5% of its surface value (~193 m), and the maximum height of sodar echoes (190–195 m), are quite close and consistent with the above definitions of the top of the SBL. Moreover, as indicated by these values, the height of the inversion layer that caps the SBL appears to lie somewhat above the height of maximum wind speed, consistent with comments by Mahrt et al. (1979).

Similarly, the height range of the RL has been defined as extending from the top of the SBL to the height of the inversion that capped the previous days mixed layer (Stull 1988). Analysis of four separate soundings from the Argonne National Laboratory's high-resolution radiosonde array in the surrounding Walnut River watershed (i.e., soundings from Beaumont, Eldorado, Leon, and Smileyburg, Kansas) show evidence of such a residual capping inversion near 1400–1600 m. Further support for this height of the RL is provided by the maximum height of concurrent echoes from NOAA's HRDL (R. Newsom 2002, personal communication).

The strong peak in Ri near 150 m in Fig. 11 clearly reflects the minimum of the shear at the jet maximum and the enhanced stability near the top of the SBL. The sharp drop in turbulence intensity around 185 m indicates that the highly stable peak in N^2 near 180 m (Fig. 10) prevents vertical coupling of the SBL turbulence below this height to higher levels. The remaining maxima in Ri within the RL at 250 and 325 m appear to be associated with fossil structures of earlier capping in-

versions as discussed by Kaimal and Finnigan (1994). We speculate that the extremely weak but sharply confined bite out in turbulence between the peaks in Ri at 250 and 325 m is a consequence of the isolation of that region from the rest of the residual layer by the stable peaks.

7. Discussion and conclusions

The results presented above provide a case study of high-resolution ''snapshots'' of some of the intriguing dynamic processes within the nighttime lower troposphere as observed above southeastern Kansas during CASES-99. The existence of an extremely sharp inversion marking the top of the SBL combined with the very steep edges of turbulence structure within the RL suggests that interpretation of these features will require considerably more study. Clearly, as discussed by Mahrt (1998), existing ''. . . concepts of stratified turbulence based on theory and laboratory results are difficult to verify in actual stratified atmospheric boundary layers.'' Toward that end, we hope that the high-resolution results obtained from the TLS technology will extend our knowledge of NBL dynamics, particularly at heights currently difficult to reach by other in situ measurement techniques.

Both the high-resolution TLS data and the HRDL vertical profiles prior to 0713 UTC have documented the existence of a low-level jet at the top of an NBL characterized by a relatively strong ground-based inversion. It is interesting to note that the height of the jet peak (120 m) reported here lies well below the typical 400-m peak discussed by Whiteman et al. (1997). Only 8% of the LLJs observed by Whiteman et al. (1997) occurred at this level. Furthermore, TLS data have also documented the subsequent breakup of this narrow LLJ, as well as the concurrent appearance of an extremely sharp temperature inversion at 180 m, that is, slightly above the height of the (earlier well defined) LLJ peak. Although the steepest portion of this temperature gradient extended for only a few centimeters, the magnitude of the gradient was determined to be in excess of 25 K m^{-1} and to retain its identity for at least 45 s (or, equivalently, over 500 m, if one assumes that the gradient seen by four turbulence probes ascending sequentially through the region was advected by the mean wind). That a similar mean gradient—albeit with slightly smaller sharp features—was observed in a subsequent flight some 20 min later suggests further that the total horizontal extent of the gradient is much larger still. We are unaware of any in situ observations of the nocturnal boundary layer inversion that would be comparable to those obtained with the TLS during CASES-99 and discussed herein.

While an interface thickness of 5 cm is small it is consistent with theoretical expectations. According to Phillips (1972), a natural scale for the thickness of an entrainment interface is the Kolmogorov length

$$l_K = (\nu^3/\varepsilon)^{1/4}, \tag{1}$$

where ν is the molecular kinematic viscosity and ε is the energy dissipation rate in the turbulent region adjacent to the interface. In our case, $\nu = 1.5 \times 10^{-5}$ m^2 s^{-1} and (see Fig. 6) $\varepsilon \approx 10^{-4}$ m^2 s^{-3}. This leads to $l_K \approx 2$ mm. If the turbulence adjacent to the interface is strongly intermittent, then between entrainment events, sharp gradients are rapidly eroded by molecular diffusion. If the interface is initially infinitely sharp and undergoes only molecular diffusion, the interface thickness D_i increases proportionally to the square root of the interface age T_i:

$$D_i = (8\kappa T_i)^{1/2} \tag{2}$$

[e.g., Eq. (8) on p. 2903 in Muschinski and Wode 1998], where κ is the molecular diffusivity of heat. The Prandtl number of air is about 0.7; therefore, $\kappa = \nu/0.7 = 2.1 \times 10^{-5}$ m^2 s^{-1}. This leads to $D_i = 1.3$ cm for $T_i = 1$ s, and $D_i = 10$ cm for $T_i = 1$ min. For $D_i = 5$ cm, we obtain $T_i = 15$ s. That is, an interface thickness of 5 cm or smaller is possible only if the interface is ''resharpened'' at least every 15 s. Muschinski and Wode (1998, p. 2905), who observed interface thickness of a few tens of centimeters in the lower free troposphere, concluded ''that sheet thickness, regardless of whether they are the remnants of Kelvin–Helmholtz instability or attributed to viscosity/thermal-conduction waves, should amount (apart from a numerical factor) to the square root of the product of molecular kinematic viscosity and a time scale that characterizes the age of a laminar sheet, the lifetime of a Kelvin–Helmholtz billow, or the period of a primary gravity wave.''

Let us assume, for the moment, that the observed 5-cm-thick interface is the edge region of a train of small-scale Kelvin–Helmholtz (KH) billows at the SBL top, such that the overturning timescale of the KH billows is $T = 7.5\, D_s/\Delta u$, where D_s is the shear layer thickness (the crest-to-trough amplitude of the KH billows), $7.5\, D_s$ is the KH billow length, and Δu is the wind speed change across the shear layer. If we further assume that the Richardson number across the shear layer is close to its traditional critical value of 0.25, we have

$$D_s = \Theta(\Delta u)^2/(4g\Delta\Theta), \tag{3}$$

where Θ is potential temperature, $g = 10$ m s^{-2} is acceleration due to gravity, and $\Delta\Theta$ is the potential temperature change across the shear layer. Inserting $\Delta u = 7.5\, D_s/T$ leads to

$$D_s = (4/15)^2(g\Delta\Theta T^2/\Theta). \tag{4}$$

With $\Theta = 300$ K, $\Delta\Theta = 1$ K, and $T = 15$ s, we find a shear layer thickness of $D_s = 53$ cm, which is about $10\, D_i$, implying a plausible ratio between edge-region thickness and shear layer thickness.

In general, the shape of the potential temperature profile suggests that the NBL can be classified as ''weakly stable'' (Mahrt 1998), with the lower SBL region dom-

inated by shear-generated turbulence and the RL above the SBL characterized by a reasonably well-mixed layer extending upward to the capping inversion. More specifically, however, our results suggest a somewhat more complex situation, with very distinct turbulent regions that exhibit strikingly different but relatively constant mean values of C_T^2 and ε within regions, and with very sharp edges at the interfaces. The change in the magnitude of both turbulent parameters at each interface is well over an order of magnitude. The lower interface appears to be closely associated with the steep positive potential temperature gradient at the top of the SBL that prevents the shear-generated turbulence below from coupling to higher heights. The turbulence interfaces at 250 and 325 m do not appear to be associated with any really significant temperature gradient or vertical velocity shear, at least on the order of that observed at the top of the SBL. This upper-level bite-out region does appear to be confined to the region bounded by two very stable narrow regions defined by enhanced Ri peaks in Fig. 11. We speculate that these peaks may be similar to the ''. . . stratified inversion layers (that) may appear and disappear above the SBL . . .'' discussed by Kaimal and Finnigan (1994). Additional pertinent comments on sustaining small values of Ri (<0.5) within thin, stably bounded layers for extended periods in the free atmosphere can be found in chapter 10.2 of Turner (1973). Other useful discussions of the relative importance of buoyancy forces and inertial forces in stratified regions can be found in Riley and Lelong (2000).

Regarding earlier published examples showing the existence of steep temperature gradients, it is interesting to compare our results with gradients found in the so-called temperature ''sheets'' first observed by high-resolution radiosondes in the atmosphere by Dalaudier et al. (1994) and further studied in the Arctic lower troposphere using a Helipod suspended beneath a helicopter by Muschinski and Wode (1998). The early work of Dalaudier et al. (1994) encompassed a much larger height range, that is, up to about 27 km in contrast to the study by Muschinski and Wode (1998) and the study reported herein that concentrated on the first kilometer of the atmosphere.

In terms of the magnitude of the observed temperature gradients, both earlier studies reported maximum observed gradients of a fraction of a Kelvin per meter, in contrast to the current results that show much steeper values. It is reasonable to assume that the difference in our results and those obtained earlier lies in the higher vertical resolution provided by TLS. This improved resolution results from the combination of a slower ascent rate (0.4 m s^{-1} for TLS in contrast to 5–7 m s^{-1} for the nontethered radiosonde or $\approx$5 m s^{-1} for Helipod) and a faster sampling rate (200 Hz for TLS in contrast to 32 Hz for the radiosonde or 100 for Helipod). For example, the vertical temperature resolution reported by Dalaudier et al. (1994) after interpolation was around 20 cm, in contrast to the maximum TLS resolution of $\sim$0.2 cm.

Dalaudier et al. (1994), using results from a series of vertically separated probes, reported that temperature steps of more than 0.3 K in the nighttime boundary layer that can extend horizontally more than 50–100 m. Our results suggest that steps of about 1 K over a few centimeters vertically can extend horizontally at least 500 m. This conclusion can be augmented to an outer limit of more than 10 km if one includes steps of 1–2 K with gradients of only 1 K m^{-1}. Similarly, in line with the earlier work, which found that such sheets were somewhat distorted vertically with a maximum distortion of typically less than about 10 m, we also find that such distortions are likely on the order of a few meters. It is important to stress, however, that while the results reported by Dalaudier et al. (1994) in the stable boundary layer can be compared directly with our results, the causal mechanism for the structures they observed at tropospheric and stratospheric heights could be considerably different than the mechanism responsible for the stable boundary layer observations.

The steep temperature gradient illustrated in Fig. 5 provides strong—if not conclusive—observational support for the possibility of enhanced ''Fresnel like'' radar echoes on both VHF and UHF wind profilers (see, e.g., Metcalf and Atlas 1973; Doviak and Zrnic 1984; Gage et al. 1985; Gossard et al. 1984; Luce et al. 1997; Muschinski and Wode 1998). It is relatively easy to demonstrate (Epstein 1930; Gossard et al. 1984) that a vertical temperature step of 1 K over a small fraction of a radar wavelength will produce an easily detectable signal on conventional VHF/UHF wind profilers. The only fundamental requirement is that the region of steep gradient be horizontally smooth on the scale of a fraction of a wavelength and extend horizontally over a Fresnel zone. A Fresnel zone at 915 MHz, a typical frequency for boundary layer radars, at heights of 100–200 m, is only a few meters. These requirements appear to be met—and in fact greatly exceeded—by the deduced horizontal dimensions of measured gradients. The primary unknown factor in this speculation is the horizontal smoothness of the surface of the temperature gradient.

Enhanced radar returns from the sharp interfaces could be interpreted incorrectly as arising from narrow regions of enhanced turbulence, that is, strong C_n^2 returns. Interestingly, in a study that discusses the origins of the well-known VHF aspect sensitivity, Woodman and Chu (1989, p. 123) discuss the existence of VHF radar echoes arising from steep vertical temperature gradients: ''According to the discussion given in the appendix, one needs temperature differences of the order of $\pm$0.5 K over a distance not much larger than a meter. We find such strong gradients impossible without the presence of turbulence.'' The observations presented here point to the existence of much steeper temperature gradients, that is, in the range of a few tens of Kelvin per meter embedded in the background turbulence. If

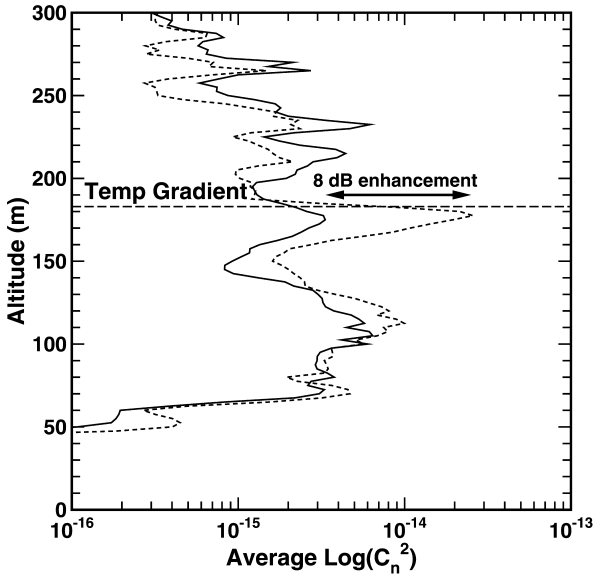

FIG. 12. Seventy-second-averaged C_n^2 vertical profiles estimated from range-corrected echo power from the FMCW radar obtained on 21 Oct 1999 beginning 0722 UTC (solid curve) and 0742 UTC (dashed curve). The 0722 UTC profile was obtained for the period when the TLS sensors detected the steep temperature gradient as they ascended through the 180–190-m altitude range. The 0742 UTC profile corresponds to the time the sensors descended through the same height range when the temperature gradient was less steep by roughly a factor of 20–30. The three maxima in signal strength at 215, 231, and 266 m are not atmospheric returns but arise from consistent antenna sidelobe echoes from surface features near the radar (S. Frasier 2002, personal communication).

we assume 1) that the above TLS observations document a reasonably common occurrence of steep temperature gradients in the RL, and 2) that the gradient surfaces are relatively smooth horizontally over Fresnel zone scales, then it follows that specular echoes can be expected to be a reasonably common occurrence in the RL on VHF and UHF returns. Indeed, since the observed gradients are significantly steeper than the ~1° values discussed in this paragraph, one can speculate that specular echoes should be observable at even higher frequencies.

Toward this end, we present in Fig. 12 preliminary evidence of an enhanced echo that was observed on the University of Massachusetts's vertically directed FMCW (2700 MHz) radar returns during the 0713–0731 UTC ascent shown in Figs. 2, 4, and 5, when the 28 K m^{-1} temperature gradient was present. This figure [data kindly provided by S. Frasier (2002, personal communication)] shows two vertical profiles of 70-s-averaged signal strength obtained using the FMCW radar for the period 0722–0742 UTC, that is, the time when the TLS instruments were passing through the 180–190-m temperature gradient during ascent and descent, respectively. The first profile (solid curve) appears similar to the subsequent profile (dotted curve) except near the ~180-m region where the steep temperature was observed. The measured difference in the echo power at this height between the two profiles is on the order of 8 dB (a factor of ~6.3), with the stronger echo present when the steepest gradients were observed. That the enhanced echo during ascent was partially due to a specular return from a steep temperature gradient is further strengthened by the fact that the TLS-observed C_n^2 profiles for the two periods differed by only about 3 dB (a factor of 2), with the earlier profile showing slightly stronger turbulence levels. Thus, it appears that the 8-dB enhancement shown at 180 m on the 0722 UTC profile could not appear to have arisen entirely from an enhanced turbulence background, but rather from a combination of both enhanced turbulence and from the very steep temperature gradient as exemplified in Fig. 5.

It is also possible to account for the echo enhancement in terms of a specular reflection from a coincident layer of enhanced humidity. According to Muschinski and Wode (1998), a comparable enhanced return would be expected from a relative humidity change of only 1% to 2% over the same 3-cm height range. In view of the 10-s (i.e., 4-m vertical sampling rate) resolution of the TLS humidity sensor, however, we are not in a position to quantify the relative contribution of a humidity change and/or a steep temperature gradient. On the other hand, the coincidence of the enhanced echo and the steep temperature gradient near 180 m suggests strongly that the temperature gradient is, at the very least, a contributing factor.

Finally, our observations appear to suggest that the observed steep temperature gradients may be causally related to ''breakdown'' of LLJ. Specifically, the steepest temperature gradient with the associated turbulence ''layering'' appears only after the disappearance of the narrow LLJ. Additional studies of TLS measurements during CASES-99, particularly if they are made in conjunction with results from other CASES-99 sensors, should clarify the general nature of this particular feature.

In summary, the TLS results presented herein represent a relatively new look at very high-resolution observations of the dynamics of the nighttime stable boundary layer. It would be interesting to find out to what extent our observational results can be reproduced with state-of-the-art direct numerical simulation (e.g., Cortesi et al. 1999; Werne and Fritts 1999) with respect to steep temperature gradients, finescale turbulence layering, and small-scale entrainment processes. The results presented here also provide an improved, higher-resolution look at turbulence processes close to interfaces, an important component of future field experiments as proposed in a recent workshop on small-scale turbulence (Muschinski and Lenschow 2001). Clearly, one of the important requirements of any future observational program would be to include higher-resolution humidity measurements to better quantify the relative

effects of steep temperature and humidity gradients on radar returns from specular surfaces.

Acknowledgments. CIRES participation in CASES-99 has been partially supported by NSF under ATM 9907289 and 01280889, by Battelle under Award DAAH04-96-C-0086 TCN 01081, and by the Army Research Office under Award DAAD 19-02-1-0435. We gratefully acknowledge useful discussions with D. C. Fritts (Colorado Research Associates), M. Jones (CIRES), and L. Mahrt (Oregon State University). Wind speed profile comparisons with R. Coulter (Argonne National Labs) are also greatly appreciated. In addition we are indebted to R. Newsom (NOAA/ETL) for help in extracting the HRDL wind profiles shown in Fig. 3 from their Web site, and especially to S. Frasier (University of Massachusetts) for providing the FMCW data used to produce Fig. 12. One of us (BBB) would like to express his appreciation to J. C. Kaimal (NOAA/ETL, retired) for providing useful insights into the dynamics of the nighttime boundary layer, and to M. Crochet (Universite de Toulon) for comments on the manuscript.

REFERENCES

Balsley, B., M. L. Jensen, and R. G. Frehlich, 1998: The use of state-of-the-art kites for profiling the lower atmosphere. *Bound.-Layer Meteor.,* **87,** 1–24.

Banta, R. M., R. K. Newsom, J. K. Lundquist, Y. L. Pichugina, R. L. Coulter, and L. Mahrt, 2002: Nocturnal low-level jet characteristics over Kansas during CASES-99. *Bound.-Layer Meteor.,* **105,** 221–252.

Bezverkhiny, V. A., A. S. Gurvich, and V. P. Kukharets, 1986: Variability of temperature fluctuation spectra in the atmospheric boundary layer. *Izv. Atmos. Oceanic Phys.,* **22,** 523–528.

——, ——, T. I. Makarova, and M. Z. Kholmyanskiy, 1988: Variation of local temperature and wind surface speed spectra in the atmospheric surface layer. *Izv. Atmos. Oceanic Phys.,* **24,** 519–527.

Blackadar, A. K., 1957: Boundary layer wind maxima and their significance for the growth of nocturnal inversions. *Bull. Amer. Meteor. Soc.,* **38,** 283–290.

Cortesi, A. B., B. L. Smith, G. Yadigaroglu, and S. Banergee, 1999: Numerical investigation of the entrainment and mixing processes in neutral and stably-stratified mixing layers. *Phys. Fluids,* **11,** 162–185.

Dalaudier, F., C. Sidi, M. Crochet, and J. Vernin, 1994: Direct evidence of ''sheets'' in the atmospheric temperature field. *J. Atmos. Sci.,* **51,** 237–247.

Doviak, R. J., and D. S. Zrnic, 1984: Reflection and scatter formula for anisotropically turbulent air. *Radio Sci.,* **19,** 325–336.

Eaton, F., S. A. McLaughlin, and J. R. Hines, 1993: A new frequency-modulated continuous-wave radar for studying planetary layer morphology. *Radio Sci.,* **30,** 75–88.

——, B. Balsley, R. Hugo, M. L. Jensen, and K. McCrae, 2000: Turbulence observations over a desert basin using a kite/tethered blimp platform. *Opt. Eng.,* **39,** 2517–2526.

Epstein, P. S., 1930: Reflection of waves in an inhomogeneous absorbing medium. *Proc. Natl. Acad. Sci.,* **16,** 627–637.

Frehlich, R. G., 1992: Laser scintillation measurements of the temperature spectrum in the atmospheric surface layer. *J. Atmos. Sci.,* **49,** 1494–1509.

——, B. Balsley, and M. L. Jensen, 1998: Atmospheric measurements of turbulence with instrumented kite platforms. *Proc. Fourth Int. Symp. on Tropospheric Profiling: Needs and Technologies,* Snowmass, CO, Radian International Electronic Systems and Cosponsors, 112–114.

——, Y. Meillier, M. L. Jensen, and B. Balsley, 2003: Turbulence measurements with the CIRES Tethered Lifting System during CASES-99: Calibration and spectral analysis of temperature and velocity. *J. Atmos. Sci.,* **60,** 2487–2495.

Gage, K. S., W. L. Ecklund, and B. B. Balsley, 1985: A modified Fresnel scattering model for the parameterization of Fresnel returns. *Radio Sci.,* **20,** 1493–1501.

Garratt, J. R., 1981: Observations in the nocturnal boundary layer. *Bound.-Layer Meteor.,* **22,** 21–48.

Gossard, E. E., W. D. Neff, R. J. Zamora, and J. E. Gaynor, 1984: The fine structure of elevated refractive layers: Implications for over-the-horizon propagation and radar sounding systems. *Radio Sci.,* **19,** 1523–1533.

Handorf, D., T. Foken, and C. Kottmeier, 1999: The stable atmospheric boundary layer over an Antarctic ice sheet. *Bound.-Layer Meteor.,* **91,** 165–189.

Jacobi, C., and R. Roth, 1995: Organisierte mesoskalige Störungen in der stabilen planetaren Grenzschicht (Organized mesoscale perturbations of the stably stratified planetary boundary layer). *Meteor. Z.,* **4,** 150–161.

Kaimal, J. C., and J. J. Finnigan, 1994: *Atmospheric Boundary Layer Flows.* Oxford University Press, 289 pp.

Kottmeier, C., 1978: Trajektorien unter Einfluß eines nächtlichen Grenzschichtstrahlstroms (Trajectories influenced by a nocturnal low-level jet). *Meteor. Rundsch.,* **31,** 129–133.

Luce, H., M. Crochet, F. Dalaudier, and C. Sidi, 1997: An improved interpretation of VHF oblique radar echoes by a direct balloon C_n^2 estimation using a horizontal pair of sensors. *Radio Sci.,* **32,** 1261–1268.

Mahrt, L., 1985: Vertical structure and turbulence in the very stable boundary layer. *J. Atmos. Sci.,* **42,** 2333–2349.

——, 1989: Intermittency of atmospheric turbulence. *J. Atmos. Sci.,* **46,** 79–95.

——, 1998: Stratified atmospheric boundary layers and breakdown of models. *Theor. Comput. Fluid Dyn.,* **11,** 263–279.

——, and N. Gamage, 1987: Observations of turbulence in stratified flow. *J. Atmos. Sci.,* **44,** 1106–1121.

——, R. C. Heald, D. H. Lenshow, B. B. Stankov, and I. B. Troen, 1979: An observational study of the structure of the nocturnal boundary layer. *Bound.-Layer Meteor.,* **17,** 247–264.

Metcalf, J., and D. Atlas, 1973: Microscale ordered motions and atmospheric structure associated with thin echo layers in stably stratified zones. *Bound.-Layer Meteor.,* **4,** 7–35.

Muschinski, A., and C. Wode, 1998: First in situ evidence for coexisting submeter temperature and humidity sheets in the lower free troposphere. *J. Atmos. Sci.,* **55,** 2893–2906.

—— and D. H. Lenschow, 2001: Future directions for research on meter- and submeter-scale atmospheric turbulence. *Bull. Amer. Meteor. Soc.,* **82,** 2831–2843.

——, R. Frehlich, M. Jensen, and B. B. Balsley, 2000: In-situ, fine-wire turbulence measurements in the nigh-time over troposphere: Connection between energy dissipation rate and temperature structure parameter. *Proc. Fifth Int. Symp. on Tropospheric Profiling: Needs and Technology,* Adelaide, Australia, Vaisala and Cosponsors, 347–349.

——, ——, ——, R. Hugo, A. Hoff, F. Eaton, and B. Balsley, 2001: Fine-scale measurements of turbulence in the lower troposphere: An intercomparison between a kite- and balloon-borne, and a helicopter-borne measurement system. *Bound.-Layer Meteor.,* **98,** 219–250.

Nieuwstadt, F. T. M., 1984a: The turbulent structure of the stable, nocturnal boundary layer. *J. Atmos. Sci.,* **41,** 2202–2216.

——, 1984b: Some aspects of the turbulent stable boundary layer. *Bound.-Layer Meteor.,* **30,** 31–55.

Oncley, S., 1999: The leading edge of turbulence instrumentation. *Air–Sea Exchange: Physics, Chemistry and Dynamics,* G. L. Geernaert, Ed., Kluwer, 49–71.

Phillips, O. M., 1972: The entrainment interface. *J. Fluid Mech.,* **51,** 97–118.

Poulos, G. S., and Coauthors, 2002: CASES-99: A comprehensive investigation of the stable nocturnal boundary layer. *Bull. Amer. Meteor. Soc.,* **83,** 555–581.

Riley, J. J., and M. P. Lelong, 2000: Fluid motions in the presence of stable stratification. *Annu. Rev. Fluid Mech.,* **32,** 613–657.

Siebert, H., M. Wendisch, T. Conrath, U. Teichmann, and J. Heintzenberg, 2003: A new balloon-borne payload for fine-scale observations in the cloudy boundary layer. *Bound.-Layer Meteor.,* **106,** 461–482.

Smedman, A.-S., 1988: Observation of a multi-level turbulence structure in a very stable atmospheric boundary layer. *Bound.-Layer Meteor.,* **44,** 231–253.

——, H. Bergstrom, and U. Hogstrom, 1995: Spectra variances and length scales in a marine stable boundary layer dominated by a low level jet. *Bound.-Layer Meteor.,* **76,** 211–232.

Stull, R. B., 1988: *An Introduction to Boundary Layer Meteorology.* Kluwer, 666 pp.

Turner, J. S., 1973: *Buoyancy Effects in Liquids.* Cambridge University Press, 367 pp.

Werne, J., and D. C. Fritts, 1999: Stratified shear turbulence: Evolution and statistics. *Geophys. Res. Lett.,* **26,** 439–442.

Whiteman, C. D., X. Bian, and S. Zhong, 1997: Low-level jet climatology for enhanced rawinsonde observations at a site in the Southern Great Plains. *J. Appl. Meteor.,* **36,** 1363–1376.

Woodman, R. F., and Y.-H. Chu, 1989: Aspect sensitivity measurements of VHF backscatter made with the Chung-Li radar: Plausible mechanisms. *Radio Sci.,* **24,** 113–125.

Wyngaard, J. C., and B. Kosovic, 1994: Similarity of structure–function parameters in the stably stratified boundary layer. *Bound.-Layer Meteor.,* **71,** 277–296.

Zilitinkevich, S. S., and D. V. Mironov, 1997: A multi-limit formulation for the equilibrium depth of a stably stratified boundary layer. *Bound.-Layer Meteor.,* **81,** 325–351.